Structures of *S. aureus* thymidylate kinase reveal an atypical active site configuration and an intermediate conformational state upon substrate binding

MASAYO KOTAKA,[1] BALVINDER DHALIWAL,[1] JINGSHAN REN,[1] CHARLES E. NICHOLS,[1] RICHARD ANGELL,[2] MICHAEL LOCKYER,[2] ALASTAIR R. HAWKINS,[3] AND DAVID K. STAMMERS[1]

[1]Division of Structural Biology, The Wellcome Trust Centre for Human Genetics, University of Oxford, Oxford OX3 7BN, United Kingdom
[2]Arrow Therapeutics, London SE1 1DA, United Kingdom
[3]Institute of Cell and Molecular Biosciences, Medical School, University of Newcastle-upon-Tyne, Newcastle-upon-Tyne NE2 4HH, United Kingdom

(RECEIVED November 29, 2005; FINAL REVISION January 10, 2006; ACCEPTED January 12, 2006)

Abstract

Methicillin-resistant *Staphylococcus aureus* (MRSA) poses a major threat to human health, particularly through hospital acquired infection. The spread of MRSA means that novel targets are required to develop potential inhibitors to combat infections caused by such drug-resistant bacteria. Thymidylate kinase (TMK) is attractive as an antibacterial target as it is essential for providing components for DNA synthesis. Here, we report crystal structures of unliganded and thymidylate-bound forms of *S. aureus* thymidylate kinase (*Sa*TMK). His-tagged and untagged *Sa*TMK crystallize with differing lattice packing and show variations in conformational states for unliganded and thymidylate (TMP) bound forms. In addition to open and closed forms of *Sa*TMK, an intermediate conformation in TMP binding is observed, in which the site is partially closed. Analysis of these structures indicates a sequence of events upon TMP binding, with helix α3 shifting position initially, followed by movement of α2 to close the substrate site. In addition, we observe significant conformational differences in the TMP-binding site in *Sa*TMK as compared to available TMK structures from other bacterial species, *Escherichia coli* and *Mycobacterium tuberculosis* as well as human TMK. In *Sa*TMK, Arg 48 is situated at the base of the TMP-binding site, close to the thymine ring, whereas a *cis*-proline occupies the equivalent position in other TMKs. The observed TMK structural differences mean that design of compounds highly specific for the *S. aureus* enzyme looks possible; such inhibitors could minimize the transfer of drug resistance between different bacterial species.

Keywords: *S. aureus*; thymidylate kinase; X-ray crystallography; substrate-induced conformational change; drug design

Staphylococcus aureus, a member of the Micrococcaceae family, is a versatile pathogen of human and various animal species. Humans are a natural reservoir of *S. aureus* (Lowy 1998), which typically lives as a commensal of the nose in 30%–70% of the population (Peacock et al. 2001). *S. aureus* is a common source of infection, causing a wide variety of diseases in humans, ranging in severity from minor skin conditions to life-threatening systemic infections such as endocarditis and haemolytic pneumonia. *S. aureus* can also cause toxin-mediated diseases such as toxic shock syndrome (Lowy 1998) and in recent years has become the most common cause of hospital-acquired

Reprint requests to: David K. Stammers, Division of Structural Biology, The Wellcome Trust Centre for Human Genetics, University of Oxford, Roosevelt Drive, Oxford OX3 7BN, UK; e-mail: daves@strubi.ox.ac.uk; fax: +44-1865-287-547.

Article published online ahead of print. Article and publication date are at http://www.proteinscience.org/cgi/doi/10.1110/ps.052002406.

infections, which are increasingly resistant to antibiotics (Peacock et al. 2001). Between 40% and 60% of *S. aureus* isolates from hospitals in several industrialized nations are now resistant to methicillin (Fluit et al. 2001). Methicillin-resistant *S. aureus* (MRSA) infections are currently treated with vancomycin; however, the emergence of vancomycin-resistant *S. aureus* (VRSA) has been reported (Hiramatsu 2001; Menichetti 2005). Thus the search for novel protein targets, against which to develop potential anti-*S. aureus* drugs, has become a priority in antibacterial research. Development of narrow-spectrum rather than broad-spectrum antibacterial agents may have some advantages in reducing the transfer of drug resistance between different bacterial species (Lee et al. 1999).

Nucleoside monophosphate (NMP) kinases are of special interest in a number of areas of drug discovery as they catalyze the production of vital precursors for the synthesis of DNA and RNA. Thymidylate kinase (TMK) (E.C. 2.7.4.9) is a member of the NMP kinase family and catalyzes the phosphoryl transfer from the preferred phosphoryl donor, ATP, to thymidine monophosphate (TMP), yielding thymidine diphosphate (TDP). The TMK reaction is positioned at the junction of the de novo and salvage pathway of thymidine triphosphate (dTTP) synthesis, with TMK being the last specific enzyme for dTTP synthesis.

NMP kinases exhibit a protein fold featuring a central five-stranded β-sheet surrounded by helices (Yan and Tsai 1999). The protein can be divided into three parts, namely, the CORE region, the NMP-binding region, and the LID region. The CORE region is the most conserved among NMP kinases, comprising mainly β-sheets with surrounding α-helices, and contains the P-loop, which is involved in the binding of ATP. The NMP-binding domain is largely helical among all NMP kinases except guanylate monophosphate kinases. The LID region is a flexible stretch of residues covering part of the phosphate donor site. Substrate-induced conformational changes have been observed in various family members of NMP kinases with large domain movements upon binding of one or both substrates (Muller-Dieckmann and Schulz 1994, 1995; Scheffzek et al. 1996; Blaszczyk et al. 2001; Sekulic et al. 2002).

Lavie et al. (1998b) identified two classes of TMKs: Class I enzymes are mainly from eukaryotes and have an arginine residue in position x_1 of the consensus sequence $Gxxx_1xGKx$ of the P-loop, which interacts with ATP; class II TMKs are of prokaryotic origin and can be distinguished by the presence of a glycine residue instead of an arginine in the x_1 position of the consensus sequence, along with additional basic residues (mostly Arg) in the LID region that interact with ATP. Inhibitors may thus potentially be designed to specifically target prokaryotic TMKs without affecting the host (human) enzyme, with the expectation that toxicity for the host can be minimized.

While structural studies on the TMP-binding site have been reported for *Mycobacterium tuberculosis* TMK (*Mt*TMK) (Li de la Sierra et al. 2001), this enzyme belongs to neither of the common classes of TMKs; rather, it appears to have a distinctive catalytic mechanism (Li de la Sierra et al. 2001; Munier-Lehmann et al. 2001; Fioravanti et al. 2003; Haouz et al. 2003). We therefore set out to study TMP binding to *S. aureus* TMK (*Sa*TMK), a class II TMK, by X-ray crystallography. *Sa*TMK exhibits typical characteristics of a class II enzyme, containing a Gly at position x_1 of the P-loop and a series of basic residues (Arg 141, 147, and 151, and Lys 144) in the LID region. This report describes the crystal structures of *Sa*TMK in its unliganded and TMP-bound states, including a form with an intermediate conformation, allowing dissection of associated sequential conformational changes of the enzyme upon TMP binding. Additionally, significant differences in the TMP site of *Sa*TMK compared to other bacterial TMKs and human TMK have been identified. The structures will thus potentially allow the design of novel inhibitors specific to *Sa*TMK, which have potential as new antimicrobial drugs to tackle the increasing problem of drug-resistant bacteria, such as MRSA.

Results and Discussion

Overall comparison of differently liganded and tagged/untagged Sa*TMK with other TMK structures*

Although the his-tagged and untagged *Sa*TMKs crystallized under similar conditions and belong to the same space group $P2_1$, the crystals have significantly different cell dimensions and varying diffraction limits (Table 1). Comparison of the structures revealed a difference in molecular packing of the TMK in the two crystal forms (data not shown). The N terminus of the untagged *Sa*TMK crystal form is close to a neighboring molecule, and thus introduction of a his-tag is presumed to be incompatible with such packing, thus producing a different form. The untagged *Sa*TMK proved to be easier to crystallize, without the need for microseeding, and the resolution of the data is also better compared to that of the tagged-form crystals. Also, differences in conformational states of TMP bound forms were observed between the his-tagged and untagged forms of the enzyme (see Table 1). In all cases, the ATP analogs and Mg^{2+} were not bound.

As expected, the overall *Sa*TMK structure has an α/β-fold consisting of nine α-helices that surround a five-stranded β-sheet core (Fig. 1A) similar to those of the

Table 1. *Data collection, refinement statistics, quality indicators, and description of SaTMK structures*

	Data set		
	1	2	3
	Unliganded Untagged	TMP bound Untagged	TMP bound His-tagged
Data collection			
X-ray source	In-house	In-house	ID 14.1, ESRF
Wavelength (Å)	1.5418	1.5418	0.934
Space group	$P2_1$	$P2_1$	$P2_1$
Unit-cell dimensions:			
a, *b*, *c* (Å)	46.3, 89.9, 50.1	45.7, 90.1, 50.3	54.5, 51.3, 72.9
α, β, γ (°)	90, 99.9, 90	90, 100.5, 90	90, 103.6, 90
Molecules per asymmetric unit	2	2	2
Resolution (Å)	30.0–2.20 (2.28–2.20)[a]	30.0–1.70 (1.76–1.70)[a]	30.0–2.30 (2.38–2.30)[a]
Completeness (%)	95.6 (78.0)	99.4 (99.4)	89.2 (49.0)
No. of reflections	66,444	207,799	54,083
No. of unique reflections	19,676	43,797	15,887
Average I/σ(I)	50.1 (18.0)	43.9 (7.1)	25.1 (4.6)
R_{merge} (%)	3.6 (8.8)	4.1 (20.9)	4.3 (24.5)
Refinement			
Reflections (working/test)	18,714/955	41,590/2190	15,082/774
R factor (R_{work}/R_{free})	0.197/0.255	0.182/0.221	0.201/0.246
No. of atoms (protein/water/others)	3084/217/9	3139/413/80	3218/101/42
Mean *B* factors (Å^2) (protein/water/others)	45.8/51.9/54.5	24.6/37.7/25.3	63.1/59.8/51.6
RMSD bond lengths (Å)	0.006	0.006	0.007
RMSD bond angles (°)	1.18	1.26	1.31
Ramachandran plot[b]			
% Residues most favored	92.7	93.2	89.6
% Additionally allowed	6.7	6.2	9.9
% Generously allowed	0	0	0
% Disallowed (residue no.)	0.6 (A92, B92)	0.6 (A92, B92)	0.6 (A92, B92)
Description			
Conformation			
(Molecule A)	Open (unliganded)	TMP site partially closed	TMP site closed
(Molecule B)	Open (unliganded)	Open with TMP bound	TMP site closed
TMP present			
(Molecule A)	No	Yes (full occupancy)	Yes (full occupancy)
(Molecule B)	No	Yes (two positions, partial occupancy)	Yes (full occupancy)
Disordered regions	A54–A55, A147–A150, A172–A176, B55, B146–B150, B172–B176	A147–A149, A173–A176, B146–B149, B172–B175	B147–B151

[a] Highest resolution shell is shown in parentheses.
[b] As defined by PROCHECK (Laskowski et al. 1993).

previously determined bacterial TMK structures, *Escherichia coli* TMK (*Ec*TMK) (Lavie et al. 1998b) and *Mt*TMK (Li de la Sierra et al. 2001) (31.6% and 21.8% amino acid identity, respectively) (Fig. 1B). Overlaying the *Ec*TMK and *Mt*TMK models in turn with *Sa*TMK resulted in an overlap of the β-sheet core with an RMSD of 0.84 Å for 34 C_αs (*Ec*TMK) and 0.70 Å for 29 C_αs (*Mt*TMK). The nine helices show more divergent positioning relative to the β-sheet (RMSD of 1.26 Å for 81 C_αs [*Ec*TMK] and 1.15 Å for 64 C_αs [*Mt*TMK]). Overlaying the *Sa*TMK structure with the human TMK structure (19% amino acid identity) (Ostermann et al. 2000), which has a similar fold to the bacterial TMKs, resulted in an overlap of the β-sheet core (RMSD of 0.47 Å for 23 C_αs) and the helices (RMSD of 1.00 Å for 78 C_αs).

In all the structures presented here, *Sa*TMK crystallizes with a dimer per asymmetric unit. The two subunits of the dimer are related by noncrystallographic twofold symmetry with helices α2, α3, and α6 stacking to their antiparallel equivalents (Fig. 1C), similar to that seen in *Ec*TMK (Lavie et al. 1997, 1998b). The dimer interface,

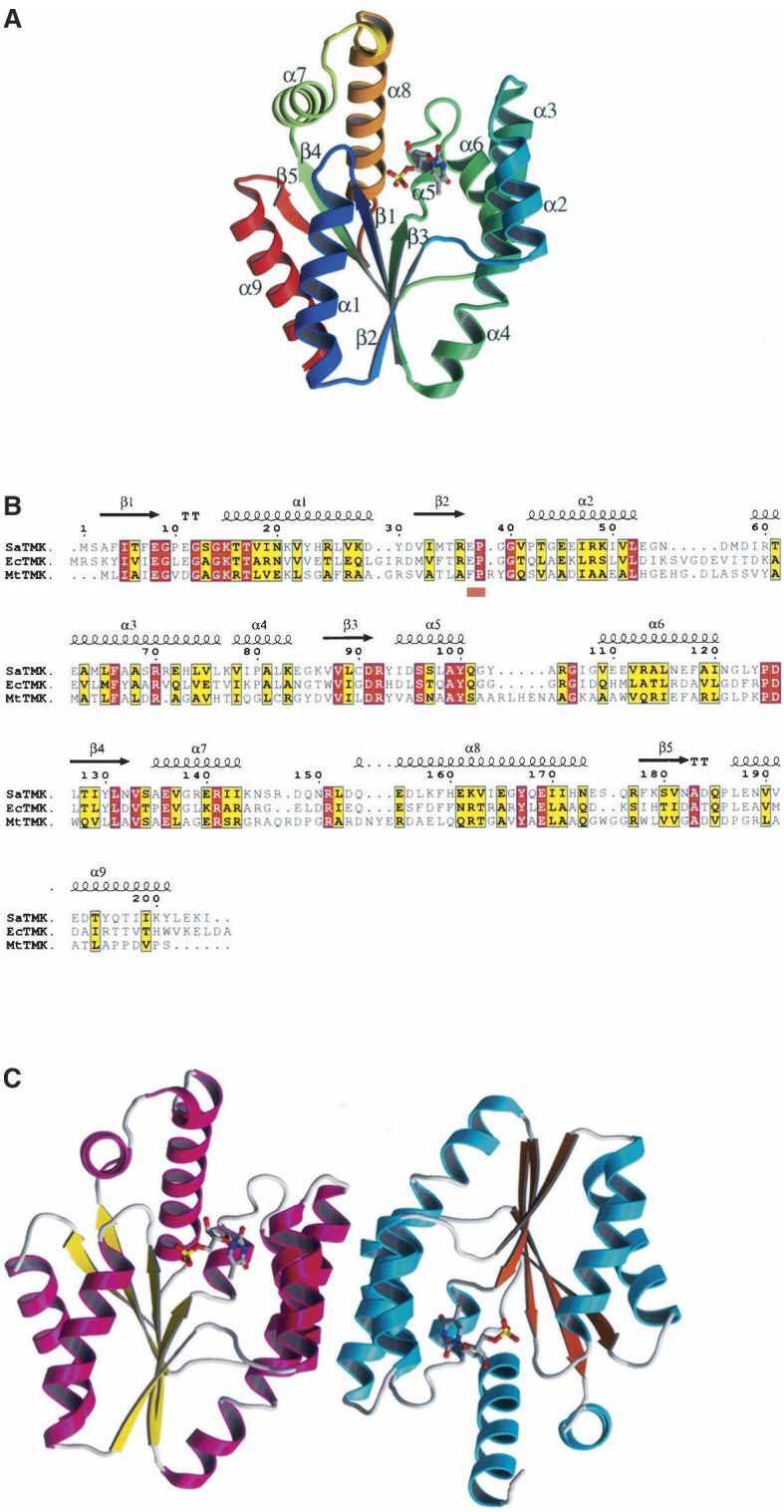

Figure 1. Structure of *Sa*TMK. (*A*) Ribbon diagram of *Sa*TMK with secondary structure marked and showing bound TMP. *Sa*TMK is shown in rainbow colors from blue at the N terminus to red at the C terminus. TMP is shown in standard atom colors, with the carbon atoms in cyan. (*B*) Sequence alignment of *Sa*TMK, *Ec*TMK, and *Mt*TMK. The secondary structure elements shown *above* the alignment are of *Sa*TMK. The orange bar *below* the alignment indicates the conserved (E/F)P loop. (*C*) Ribbon diagram of the *Sa*TMK dimer. The helices of the two molecules are shown in magenta and cyan, while the sheets are shown in yellow and orange. TMP is shown in standard atom colors, with the carbon atoms in gray.

although largely hydrophobic, also contains two pairs of hydrogen bonding interactions, Asp 58–Arg 71 and Arg 60–Asn 121, which are not observed in other TMK structures. Arg 92 of the conserved DRx loop is the only residue lying outside the allowed regions of the Ramachandran plot. Pro 38 of the conserved sequence (E/F)P is in a *cis* conformation, as in previously reported TMK structures (Lavie et al. 1997, 1998a,b; Ostermann et al. 2000, 2003; Li de la Sierra et al. 2001).

Comparing the three different *Sa*TMK structures determined here shows conformational differences in the region of helices α2 and α3. Molecule A of the unliganded, untagged *Sa*TMK superimposed on that of TMP-bound his-tagged *Sa*TMK (Table 2), with the exception of the TMP-binding site and the LID region. Displacement of α2 and α3 at the TMP-binding domain was observed with unliganded *Sa*TMK adopting a more open conformation than TMP-bound his-tagged TMK and the LID region being in the open conformation. We therefore designate the unliganded/untagged and his-tagged/TMP-bound *Sa*TMK structures as the open and TMP site closed conformations, respectively (Table 1), and superposition of molecule A of the two *Sa*TMK structures indicates that a rotation of 17.8° of molecule B has occurred. This rotation is a concerted movement of the dimer resulting from the movement of α2 and α3 as there are no significant changes in the interactions across the dimer interface. Comparison of the TMP-bound untagged *Sa*TMK structure with the open and TMP site closed conformations of *Sa*TMK revealed that molecule B has the open conformation while molecule A has an intermediate conformation (Table 2), which we designate as TMP site partially closed (Table 1). Such conformational changes are related to the presence or absence of TMP as well as the presence or absence of the his-tag and are discussed in more detail in the following sections.

Comparison of the TMP-binding site in different TMKs

No ligands were seen to be bound in the untagged *Sa*TMK structure despite the enzyme being crystallized in the presence of substrates, while for the his-tagged *Sa*TMK structure, TMP was observed in both molecules with full occupancy (Table 1). It did, however, prove possible to bind TMP to untagged *Sa*TMK by soaking in high concentrations of TMP, where it is observed in the expected site in molecule A with full occupancy. For molecule B, TMP is found in two positions, both with partial occupancy (Table 1), which appears to be in part due to the crystal packing of the untagged *Sa*TMK molecules such that the substrate site in molecule B is held more in the open conformation by contacts with a neighboring molecule.

Analysis of TMP binding shows that, although some features are in common with other TMKs, a significant difference in one region of the binding site is apparent. The TMP-binding site of *Sa*TMK and the associated network of hydrogen bonds are shown in Figure 2A. The features in common for TMP binding among different TMKs are (1) aromatic ring stacking interactions of the pyrimidine ring and a phenylalanine side chain (in this case Phe 66); (2) the positioning of Tyr 100, which allows selection of deoxynucleotides over ribonucleotides; and (3) an H-bond between O4 of the pyrimidine moiety of TMP and the side chain of Arg 70, which favors the selection of T/U over C. The importance of the interaction of Arg 70 to O4 of the thymine base of TMP is demonstrated in the equivalent residues of varicella zoster virus thymidine kinase (Bird et al. 2003) and Herpes simplex virus type 1 thymidine kinase (Hinds et al. 2000; Vogt et al. 2000). Other residues that are <3.9 Å away from TMP include Glu 11, Lys 15, Arg 36, Glu 37, Arg 92, Ser 97, and Gln 101. The interaction of the P-loop carboxylic residue Glu 11 with the ribose 3′-OH of TMP is conserved in all TMKs, an essential interaction for locating the sugar ring. O3 of the TMP phosphate group interacts with NE of Arg 92; the latter is the only residue to have a "disallowed" conformation in the enzyme structure. Arg 92 has been shown to be important for the phosphoryl transfer from the donor to TMP (Haouz et al. 2003).

Table 2. *Comparison of different* Sa*TMK structures*

Molecule 1 (conformation)	Molecule 2 (conformation)	RMSD (equivalenced C_αs)
1A[a] (Open [unliganded])	1B (Open [unliganded])	0.37 Å (189)
2A (TMP-site partially closed)	2B (Open with TMP bound)	0.53 Å (191)
3A (TMP-site closed)	3B (TMP site closed)	0.26 Å (194)
1A (Open [unliganded])	3A (TMP site closed)	0.57 Å (181)
1A (Open [unliganded])	2A (TMP site partially closed)	0.46 Å (190)
1A (Open [unliganded])	2B (Open with TMP bound)	0.39 Å (193)
2A (TMP-site partially closed)	3A (TMP site closed)	0.46 Å (185)

[a] Data set and molecule with reference to Table 1.

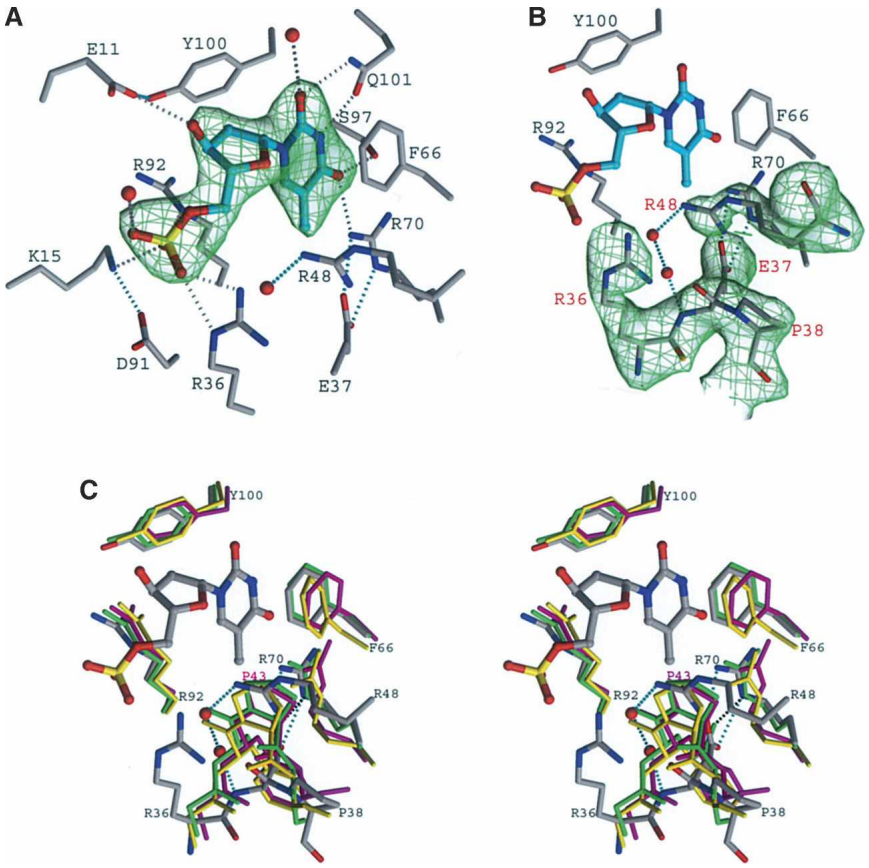

Figure 2. TMP-binding site of *Sa*TMK. (*A*) Simulated annealing omit map of bound TMP in his-tagged *Sa*TMK structure. Carbon atoms of TMP are drawn in cyan; those of residues interacting with TMP are drawn in gray. Potential hydrogen bonds are indicated by dotted lines; those that directly involve atoms of the substrate are drawn in gray, others in cyan. (*B*) Simulated annealing omit map of the (E/F)P loop and Arg 48 in his-tagged *Sa*TMK structure. Carbon atoms of TMP are drawn in cyan; those of residues of *Sa*TMK are drawn in gray. (*C*) Stereo view of the superposition of the TMP-binding site of *Sa*TMK, *Ec*TMK, *Mt*TMK, and human TMK. The important residues defining the TMP-binding site and the positions of the conserved *cis*-proline are shown. The residues of *Sa*TMK and TMP are drawn in atom colors, while the residues of *Ec*TMK, *Mt*TMK, and human TMK are drawn in green, yellow, and magenta, respectively. The residues of *Sa*TMK are labeled in black, and the *cis*-Pro 43 of human TMK is labeled in magenta. Interaction of Arg 48 with the main-chain N atom of Glu 37 via water molecules and the interaction of Glu 37 with Arg 70 are indicated by cyan dotted lines. The interaction of Glu 40 with Arg 74 of *Ec*TMK is indicated by black dotted lines.

Turning to the areas of significant difference in the TMP-binding site of *Sa*TMK when compared to those in *Ec*TMK, *Mt*TMK, and human TMK: Besides the conserved interaction with the thymine base of TMP discussed above, Arg 70 of *Sa*TMK also interacts with OD1 of Asn 116 via atom NH1. A similar interaction is observed in *Mt*TMK and human TMK, where the equivalent residue, Arg 74 (Arg 76 in human TMK), forms an ion pair with Glu 124 (Asp 121 in human TMK), while in *Ec*TMK it is replaced by interactions with Tyr 75 and Asp 102. Arg 70 NE and NH2 atoms form salt bridge/H-bonds with the carboxylate group of Glu 37, also observed in *Ec*TMK; however, the interaction cannot be present with the structurally equivalent phenylalanine in both *Mt*TMK and human TMK. While the thymidine N3 and O2 atoms H-bond with Gln 101 in *Sa*TMK and *Ec*TMK, for *Mt*TMK the O2 of the TMP base does not form a contact with the protein and N3 interacts with an asparagine residue (Asn 100). In human TMK, the thymidine N3 and O3 atoms do not form direct contacts with the protein but interact with Thr 105 via water molecules. Apart from the interaction with Arg 70 discussed previously, the O4 of the TMP pyrimidine ring also H-bonds with Ser 97; this interaction is replaced by a threonine (Thr 105) in *Ec*TMK and an arginine (Arg 74) in *Mt*TMK, while in human TMK, this interaction is not observed since the equivalent residue is a glycine (Gly 102). Besides interaction with Arg 92, the O3 of the TMP base in *Sa*TMK also forms an H-bond with the conserved Lys 15, an interaction not

observed in other reported TMK structures. For example, in the *Ec*TMK structure with the bisubstrate inhibitor TP_5A, Lys 16 H-bonds with the β- and γ-phosphates of the phosphoryl donor (Lavie et al. 1998b), while in *Mt*TMK, the equivalent lysine (Lys 13) interacts with the β-phosphate (Fioravanti et al. 2003). This conserved lysine is thought to have a catalytic role of stabilizing the pentavalent transition state involving the phosphoryl group to be transferred (Reinstein et al. 1990). The conserved lysine also plays an important role in maintaining the conformation of the P-loop, as suggested by site-directed mutagenesis in shikimate kinase (Krell et al. 2001) and adenylate kinase (Reinstein et al. 1990; Tian et al. 1990; Byeon et al. 1995). Arg 36 interacts with O1 of the TMP phosphate group, but this interaction is replaced by Tyr 39 in *Mt*TMK and Arg 51 in *Ec*TMK (equivalent of Arg 48 in *Sa*TMK). Unlike Arg 51 of *Ec*TMK, Arg 48 does not interact with TMP; instead, it takes the place of Pro 38 to form the bottom of the TMP-binding cavity.

The most striking difference in the substrate-binding site of *Sa*TMK, compared with other TMKs, is at the base of the TMP-binding cavity. In all other reported TMK structures, the loop containing the conserved (E/F)P sequence, which has proline in a *cis* conformation and connects β2 to α2, forms the base of the TMP-binding cavity (Lavie et al. 1997, 1998a,b; Ostermann et al. 2000; Li de la Sierra et al. 2001). The main-chain N atom of the *cis*-proline is positioned ~4 Å from the pyrimidine group of TMP. In contrast, in *Sa*TMK, Arg 36 forms part of the turn containing the conserved (E/F)P sequence (Fig. 2B) rather than being in at the end of β2, as is the case for *Ec*TMK, *Mt*TMK, and human TMK. Although the conserved Glu 37 of *Sa*TMK still interacts with Arg 70, as is also observed in *Ec*TMK, the *cis*-proline has turned away from the TMP-binding site and is located ~7.6 Å from the bound TMP, creating a space at the base of the TMP-binding site. The additional space is filled by the side chain of Arg 48 (Fig. 2C), which, in turn, is linked to the main-chain nitrogen atom of Glu 37 of the (E/F)P loop via water molecules.

TMP-induced conformational changes

As described in a previous section, a range of conformations of *Sa*TMK have been identified that are related to TMP binding (Table 1). The structures appear to represent snapshots along the TMP-binding pathway of *Sa*TMK (Fig. 3A). Combining SHP and HINGEFIND analyses from open and TMP site closed conformations revealed an overall domain movement of helices α2 and α3 (residues 43–75) toward the CORE region at the TMP-binding site with a rotation of ~14° (Fig. 3A). However, from analysis of torsion angle difference (TAD) plots, no hinge points relating to the domain movement were identified. In spite of this, the TAD plot showed significant torsion angle differences at the loop connecting α2 and α3 (residues 51–60) (Fig. 3B), which is flexible as indicated by the high *B*-factors.

Movement of the LID region toward the CORE region of the enzyme was also evident upon TMP binding, involving the rotation of the LID domain by 31°, with hinge points at residue 142 and residue 158 (Fig. 3A,B). This change results in the enzyme adopting a closed conformation with respect to the TMP site, as observed in other NMP kinases upon the binding of the non-ATP substrate (Vonrhein et al. 1995; Lavie et al. 1997; Briozzo et al. 1998; Fioravanti et al. 2003; Segura-Pena et al. 2004).

Closer analysis of the differences at the TMP-binding site from open to closed conformations revealed that the changes involved sequential movements of α3 and α2 toward the TMP-binding site. Upon TMP binding, helix α3 rotates by 4.3° toward the CORE region with little movement of α2, as seen in the transition from the open to TMP site partially closed conformation (Fig. 3A). Helix α2 then rotates toward the CORE region by 16.5°, closing the TMP-binding site. The extent of movement can also be expressed by the shift of the C_α positions of residues 53 and 58, which are located at the beginning and the end of the loop connecting the helices α2 and α3, respectively. The movement of the C_α of residue 58 is 0.67 Å between open and TMP site partially closed conformations and 0.92 Å between open and TMP site closed conformations, while residue 53 moves 1.4 Å between open and TMP site partially closed conformations and 4.7 Å between open and TMP site closed conformations.

The superposition of the open, partially closed, and closed conformations of the TMP-binding site of *Sa*TMK is illustrated in Figure 3C. In the open conformation, a network of water molecules interacting with residues Gln 101 and Arg 70 occupies the thymine portion of the TMP site. Upon TMP binding, the rotation of helix α3 allows the stacking of Phe 66 to the pyrimidine ring of TMP, and although the site remains partially open, the essential features of TMP binding are established at this stage. The movement of α2 then brings Arg 48 to assume its position at the bottom of the TMP-binding cavity, thereby closing the TMP-binding site. Accompanying small induced-fit movements of helix α3 along with residues 11 and 36 also occur.

Substrate-induced conformational changes at the NMP-binding site have been observed in the other members of the NMP kinase family, e.g., human UMP/CMP kinase (Segura-Pena et al. 2004), yeast GMP kinase (Stehle and Schulz 1990; Blaszczyk et al. 2001), adenylate kinases (Vonrhein et al. 1995), and *E. coli* CMP kinase (Briozzo

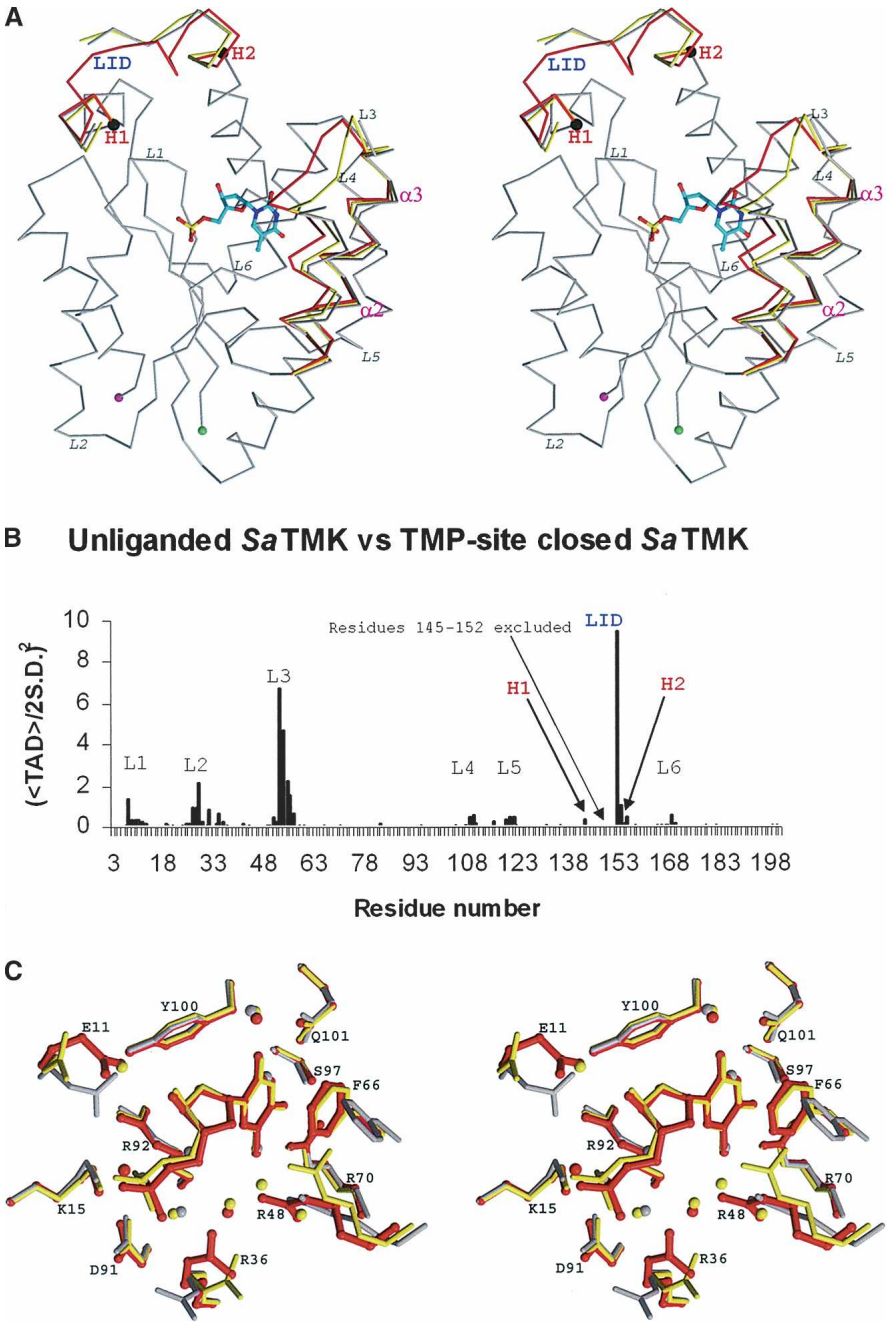

Figure 3. TMP-induced conformational change of *Sa*TMK. (*A*) Stereo view of the alignment of Cα traces of unliganded *Sa*TMK (gray); TMP site partially closed *Sa*TMK (yellow) and TMP site closed *Sa*TMK (red). The N and C termini are indicated by green and by magenta spheres, respectively. The helices α2 and α3 are labeled in magenta. Hinge points of the LID regions (labeled in blue) as identified with TAD analysis are drawn as black spheres and labeled in red. Flexible loops with torsion angle differences identified by TAD analysis are labeled in italics. (*B*) TAD plot of comparison of torsion angles between unliganded and TMP site closed *Sa*TMK. The significant TAD peaks are labeled in black and correspond to the loops in *A*. The LID region is labeled in blue. The hinge points of the LID region are labeled as H1 and H2 in red. (*C*) Close-up stereo view of TMP-binding site. Residues are drawn in gray for unliganded *Sa*TMK, in yellow for the *Sa*TMK with partially closed TMP site, and in red for TMP site closed *Sa*TMK.

et al. 1998). However, the current report is the first description of substrate-induced conformational changes in TMK upon TMP binding in a class I or II TMK, as prior to this no unliganded structures had been solved. In *Mt*TMK, which is distinctive to class I or II, only a small induced-fit mechanism at the level of the α-phosphate group and the

ribose moiety upon TMP-binding has been reported (Fioravanti et al. 2003). This small difference can be explained, as the (E/F)P loop of *Mt*TMK is already in position to form the base of the TMP-binding cavity. In this case, the TMP-binding site is already pre-tuned to accommodate the substrate, and therefore no major domain movement is required to close the binding site. However, as the base of the TMP-binding site is in a more open conformation than that of *Mt*TMK and other bacterial TMKs (Fig. 2C), movement of helix α2 is required to bring Arg 48 into position to close the TMP-binding site. The TMP-induced conformational change observed in *Sa*TMK therefore appears to be related to the position of the (E/F)P loop.

Conclusion

*Sa*TMKs with differing conformational states were observed from crystal structure determination of his-tagged and untagged *Sa*TMK together with the presence or absence of TMP. Differences in molecular packing between crystals of tagged and untagged forms of *Sa*TMK appear to contribute to the observed range of conformational states. The crystal contacts at the TMP-binding site of untagged *Sa*TMK crystal forms are more extensive than those of the his-tagged form, resulting in a hindrance of domain movement upon TMP binding. Analysis of the structures reveals sequential conformational changes from an open TMP-binding site to a closed state.

Significant differences in the conformation of the TMP-binding site in *Sa*TMK compared to known bacterial and human TMK structures were identified that mainly relate to the positioning of the (E/F)P loop. Such differences are surprising considering the level of sequence identity particularly between *Sa*TMK and *Ec*TMK (~32%), typical class II TMKs, and the conserved role of substrate binding central to the biological function of these enzymes. The structural results appear unambiguous as the TMP site conformation was observed in both crystal forms of untagged and his-tagged *Sa*TMK. It is clear that prediction of the TMP-binding site of *Sa*TMK from homology modeling would be difficult, thus re-emphasising the need for caution in using such approaches.

The availability of crystal structures of TMP binding to *Sa*TMK should stimulate the design of inhibitors that may have potential as novel antibacterial drugs using structure-based approaches. Two options to target the TMP-binding site of the enzyme are possible. First, to direct the design of inhibitors to regions of the TMP site conserved between the various bacterial TMKs but with structural differences to that of human TMK in order to obtain broad spectrum antibacterial agents. A second, more intriguing, option is to target the region with a conformational difference in the TMP-binding site of *Sa*TMK with the aim of developing narrow-spectrum inhibitors against MRSA. One possibility would be to design inhibitors containing hydrogen-bonding groups targeting Arg 48 at the base of the TMP-binding cavity of *Sa*TMK, an interaction not formed by other TMKs containing proline in this position of the active site. Such inhibitors would have the advantage of minimizing the transfer of drug resistance between different bacterial species as well as having the potential to minimize binding to the host (human) enzyme, hence minimizing toxicity.

Materials and methods

Cloning, protein expression, and purification

The gene for *Sa*TMK was amplified by PCR from *S. aureus* (strain SH1000) genomic DNA using primers incorporating NdeI/BamHI restriction sites, and the product was ligated into the expression plasmid pET15b (Novagen). The resulting plasmid, pMUT68 coding for N-terminal his-tagged *Sa*TMK, was transformed into the *E. coli* expression strain Codon$^+$. For untagged *Sa*TMK, the PCR product was ligated into the expression plasmid pET3a (Novagen) via the NdeI and BamHI sites. The resulting plasmid, pMUT111, was transformed into the expression strain BL21(DE3). For both constructs, cells were grown at 37°C in LB with ampicillin selection and induced with IPTG for 5 h. Typically, 25 g of pelleted cells was sonicated in 500 mL of 50 mM K phosphate (pH 7.2), 1 mM DTT, and 1 mM benzamidine, and the lysate was clarified by centrifugation.

His-tagged *Sa*TMK was purified using two column chromatography steps: (1) Zn^{2+}-charged chelating Sepharose column eluted with a 0.0–0.3 M imidazole gradient in 50 mM K phosphate (pH 7.2) and 1 mM DTT, and (2) hydroxyapatite column eluted with a 50–400 mM gradient of K phosphate (pH 7.2) and 1 mM DTT. At each step in the purification procedure, fractions were analyzed by SDS-PAGE and appropriate fractions were pooled, giving a final yield of ~500 mg of *Sa*TMK.

Untagged *Sa*TMK was purified in a six-step protocol as follows: (1) DEAE Sephacel chromatography eluted with a 0.0–1.0 M NaCl gradient in 50 mM K phosphate (pH 7.2) and 1 mM DTT; (2) ammonium sulfate fractionation (35%–55% saturation); (3) phenyl-Sepharose eluted with a 1.0–0.0 M ammonium sulfate gradient in 50 mM K phosphate (pH 7.2) and 1 mM DTT; (4) hydroxyapatite chromatography in which the protein eluted following washes of 50 mM K phosphate (pH 7.2) and 1 mM DTT; (5) Mono Q FPLC eluted with a 0.0–1.0 M NaCl gradient in 50 mM K phosphate (pH 7.2) and 1 mM DTT; and (6) Sephacryl S300 gel-filtration chromatography run in 150 mM NaCl, 50 mM K phosphate (pH 7.2), and 1 mM DTT. At each step in the purification procedure, fractions were analyzed by SDS-PAGE, and appropriate fractions were pooled. The final yield was ~70 mg of purified untagged *Sa*TMK. For both untagged and his-tagged *Sa*TMK, protein was concentrated and buffer exchanged into 20 mM Tris-HCl (pH 7.4), 150 mM KCl using Vivaspin centrifugal concentrators (Vivascience) prior to crystallization.

Crystallization

For his-tagged *Sa*TMK, an initial crystallization screen was performed using protein at 22 mg/mL complexed with 5 mM

TMP, 5 mM ATPγS. Drops (100 nL) of protein solution were mixed with 100 nL of screening solution in a sitting drop vapor diffusion plate using a Cartesian robot (Walter et al. 2005). Crystals were obtained at 291 K from Hampton Grid Screen PEG/LiCl condition D4 (1 M LiCl, 0.1M HEPES at pH 7.0, 30% PEG 6000). Optimization of the condition gave crystals from 1 M LiCl, 0.1 M Na Cacodylate (pH 6.2–6.8), and 16%–22% PEG 6000; the best crystals were obtained by micro-seeding. Screening conditions for the crystallization of untagged *Sa*TMK yielded crystals from 1 M LiCl, 0.1M HEPES (pH 6.8–7.2), and 16%–20% PEG 3350. For TMP bound untagged *Sa*TMK structure, crystals were soaked in mother liquor containing 25 mM TMP, 25 mM AMPPcP, and 25 mM $MgCl_2$ for 1 h prior to data collection.

Data collection and structure determination

The his-tagged and untagged *Sa*TMK crystals were flash-cooled to 100 K after the addition of 10% MPD and 10% ethylene glycol to the mother liquor. For the his-tagged *Sa*TMK crystals, data were collected on beamline ID 14.1 at the ESRF (Grenoble, France), while data for the untagged crystals were collected in-house using Cu Kα radiation from a Rigaku MicroMax 007 generator equipped with a MAR345 image plate. Data were processed with the HKL suite of programs (Otwinowski and Minor 1997). Crystals all belonged to space group $P2_1$ but with two distinct sets of cell dimensions dependent on the presence or absence of the his-tag. Data collection and processing statistics are shown in Table 1. Molecular replacement used a combination of *Ec*TMK (PDB accession no. 4TMK) (Lavie et al. 1998b) and *Mt*TMK structures (PDB accession no. 1GSI) (Li de la Sierra et al. 2001). The two TMK dimers were superimposed with the program SHP (Stuart et al. 1979), and structure factors were calculated from the overlapped models, which were used to solve the his-tagged *Sa*TMK structure by molecular replacement with CNS (Brünger et al. 1998). O (Jones et al. 1991) was used for model building with *Ec*TMK as the starting model. The untagged *Sa*TMK structures were solved by molecular replacement with coordinates of the refined his-tagged *Sa*TMK model using CNS (Brünger et al. 1998). The structures were refined in CNS using simulated annealing, positional, and *B*-factor refinement to give the final statistics shown in Table 1. O was used for model rebuilding (Jones et al. 1991).

Structure and sequence alignments

For comparison of the *Sa*TMK structure with *Mt*TMK, *Ec*TMK, and human TMK (PDB accession no. 1E2F), SHP was used to overlap pairs of protein structures (Stuart et al. 1979). Different TMK amino acid sequences were retrieved via the ExPASy proteomics server Web site (http://www.expasy.org) and aligned with ClustalW.

Model analysis and identification of conformational changes

The *Sa*TMK models were evaluated using PROCHECK (Laskowski et al. 1993). Different *Sa*TMK structures were compared by overlapping coordinates sets using SHP (Stuart et al. 1979). Residues of *Sa*TMK <3.9 Å away from TMP were determined by using the program CONTACT (Collaborative Computational Project, Number 4 1994). C_α torsion angles for each residue i, defined as the dihedral angle $C_\alpha(i-1)-C_\alpha(i)-C_\alpha(i+1)-C_\alpha(i+2)$, were examined for each *Sa*TMK structure according to methods described by Flocco and Mowbray (1995). Torsion angle differences (TAD) between the structures were plotted using EXCEL with the *Y*-axis as $(\langle TAD\rangle/2\times SD)^2$, which allows significant TAD peaks to be observed above noise (Nichols et al. 2004). The locations of the hinges were found using the TCL script HINGEFIND (Wriggers and Schulten 1997) (partition value = 1.1 and maximum domains = 10), run, and visualized with the graphics package VMD (Humphrey et al. 1996).

Preparation of figures

The figures were prepared using BOBSCRIPT (Kraulis 1991; Esnouf 1999) and rendered with RASTER3D (Merritt and Bacon 1997).

Coordinates

The coordinates and structure factors have been deposited in the Protein Data Bank (accession nos. 2CCK, 2CCJ, and 2CCG, for the unliganded untagged, TMP bound untagged, and TMP bound his-tagged *Sa*TMKs, respectively).

Acknowledgments

We thank the staff at beamline ID14.1 at the ESRF, Grenoble for help with the data collection; Dr. R. Esnouf, Ms. J. Dong, and Mr. A. Tamer for computer support; and Dr. K. Harlos for assistance with the in-house data collection. We thank Arrow Therapeutics for funding the research at Newcastle and at Oxford.

References

Bird, L.E., Ren, J., Wright, A., Leslie, K.D., Degreve, B., Balzarini, J., and Stammers, D.K. 2003. Crystal structure of varicella zoster virus thymidine kinase. *J. Biol. Chem.* **278:** 24680–24687.

Blaszczyk, J., Li, Y., Yan, H., and Ji, X. 2001. Crystal structure of unligated guanylate kinase from yeast reveals GMP-induced conformational changes. *J. Mol. Biol.* **307:** 247–257.

Briozzo, P., Golinelli-Pimpaneau, B., Gilles, A.M., Gaucher, J.F., Burlacu-Miron, S., Sakamoto, H., Janin, J., and Barzu, O. 1998. Structures of *Escherichia coli* CMP kinase alone and in complex with CDP: A new fold of the nucleoside monophosphate binding domain and insights into cytosine nucleotide specificity. *Structure* **6:** 1517–1527.

Brünger, A.T., Adams, P.D., Clore, G.M., DeLano, W.L., Gros, P., Grosse-Kunstleve, R.W., Jiang, J.S., Kuszewski, J., Nilges, M., Pannu, N.S., et al. 1998. Crystallography & NMR system: A new software suite for macromolecular structure determination. *Acta Crystallogr. D Biol. Crystallogr.* **54:** 905–921.

Byeon, L., Shi, Z., and Tsai, M.D. 1995. Mechanism of adenylate kinase. The "essential lysine" helps to orient the phosphates and the active site residues to proper conformations. *Biochemistry* **34:** 3172–3182.

Collaborative Computational Project, Number 4. 1994. The CCP4 suite: Programs for protein crystallography. *Acta Crystallogr. D Biol. Crystallogr.* **50:** 760–763.

Esnouf, R.M. 1999. Further additions to MolScript version 1.4, including reading and contouring of electron-density maps. *Acta Crystallogr. D Biol. Crystallogr.* **55:** 938–940.

Fioravanti, E., Haouz, A., Ursby, T., Munier-Lehmann, H., Delarue, M., and Bourgeois, D. 2003. *Mycobacterium tuberculosis* thymidylate kinase: Structural studies of intermediates along the reaction pathway. *J. Mol. Biol.* **327:** 1077–1092.

Flocco, M.M. and Mowbray, S.L. 1995. Cα-based torsion angles: A simple tool to analyze protein conformational changes. *Protein Sci.* **4:** 2118–2122.

Fluit, A.C., Verhoef, J., and Schmitz, F.J. 2001. Frequency of isolation and antimicrobial resistance of Gram-negative and Gram-positive bacteria from patients in intensive care units of 25 European university hospitals participating in the European arm of the SENTRY Antimicrobial Surveillance Program 1997–1998. *Eur. J. Clin. Microbiol. Infect. Dis.* **20:** 617–625.

Haouz, A., Vanheusden, V., Munier-Lehmann, H., Froeyen, M., Herdewijn, P., Van Calenbergh, S., and Delarue, M. 2003. Enzymatic and structural analysis of inhibitors designed against *Mycobacterium tuberculosis* thymidylate kinase. New insights into the phosphoryl transfer mechanism. *J. Biol. Chem.* **278:** 4963–4971.

Hinds, T.A., Compadre, C., Hurlburt, B.K., and Drake, R.R. 2000. Conservative mutations of glutamine-125 in herpes simplex virus type 1 thymidine kinase result in a ganciclovir kinase with minimal deoxypyrimidine kinase activities. *Biochemistry* **39:** 4105–4111.

Hiramatsu, K. 2001. Vancomycin-resistant *Staphylococcus aureus*: A new model of antibiotic resistance. *Lancet Infect. Dis.* **1:** 147–155.

Humphrey, W., Dalke, A., and Schulten, K. 1996. VMD: Visual molecular dynamics. *J. Mol. Graph.* **14:** 33–38.

Jones, T.A., Zou, J.Y., Cowan, S.W., and Kjeldgaard, M. 1991. Improved methods for building protein models in electron density maps and the location of errors in these models. *Acta Crystallogr. A* **47:** 110–119.

Kraulis, P.J. 1991. MOLSCRIPT: A program to produce both detailed and schematic plots of protein structures. *J. Appl. Crystallogr.* **24:** 946–950.

Krell, T., Maclean, J., Boam, D.J., Cooper, A., Resmini, M., Brocklehurst, K., Kelly, S.M., Price, N.C., Lapthorn, A.J., and Coggins, J.R. 2001. Biochemical and X-ray crystallographic studies on shikimate kinase: The important structural role of the P-loop lysine. *Protein Sci.* **10:** 1137–1149.

Laskowski, R.A., MacArthur, M.W., Moss, D.S., and Thornton, J.M. 1993. PROCHECK: A program to check the stereochemical quality of protein structures. *J. Appl. Crystallogr.* **26:** 283–291.

Lavie, A., Vetter, I.R., Konrad, M., Goody, R.S., Reinstein, J., and Schlichting, I. 1997. Structure of thymidylate kinase reveals the cause behind the limiting step in AZT activation. *Nat. Struct. Biol.* **4:** 601–604.

Lavie, A., Konrad, M., Brundiers, R., Goody, R.S., Schlichting, I., and Reinstein, J. 1998a. Crystal structure of yeast thymidylate kinase complexed with the bisubstrate inhibitor P1-(5′-adenosyl) P5-(5′-thymidyl) pentaphosphate (TP5A) at 2.0 Å resolution: Implications for catalysis and AZT activation. *Biochemistry* **37:** 3677–3686.

Lavie, A., Ostermann, N., Brundiers, R., Goody, R.S., Reinstein, J., Konrad, M., and Schlichting, I. 1998b. Structural basis for efficient phosphorylation of 3′-azidothymidine monophosphate by *Escherichia coli* thymidylate kinase. *Proc. Natl. Acad. Sci.* **95:** 14045–14050.

Lee, V.J., Miller, G.H., and Yagisawa, M. 1999. What's new in the antibiotic pipeline. *Curr. Opin. Microbiol.* **2:** 475–482.

Li de la Sierra, I., Munier-Lehmann, H., Gilles, A.M., Barzu, O., and Delarue, M. 2001. X-ray structure of TMP kinase from *Mycobacterium tuberculosis* complexed with TMP at 1.95 Å resolution. *J. Mol. Biol.* **311:** 87–100.

Lowy, F.D. 1998. *Staphylococcus aureus* infections. *N. Engl. J. Med.* **339:** 520–532.

Menichetti, F. 2005. Current and emerging serious Gram-positive infections. *Clin. Microbiol. Infect.* **11 (Suppl. 3):** 22–28.

Merritt, E.A. and Bacon, D.J. 1997. Raster3D: Photorealistic molecular graphics. *Methods Enzymol.* **277:** 505–524.

Müller-Dieckmann, H.J. and Schulz, G.E. 1994. The structure of uridylate kinase with its substrates, showing the transition state geometry. *J. Mol. Biol.* **236:** 361–367.

———. 1995. Substrate specificity and assembly of the catalytic center derived from two structures of ligated uridylate kinase. *J. Mol. Biol.* **246:** 522–530.

Munier-Lehmann, H., Chaffotte, A., Pochet, S., and Labesse, G. 2001. Thymidylate kinase of *Mycobacterium tuberculosis*: A chimera sharing properties common to eukaryotic and bacterial enzymes. *Protein Sci.* **10:** 1195–1205.

Nichols, C.E., Dhaliwal, B., Lockyer, M., Hawkins, A.R., and Stammers, D.K. 2004. High-resolution structures reveal details of domain closure and "half-of-sites-reactivity" in *Escherichia coli* aspartate β-semialdehyde dehydrogenase. *J. Mol. Biol.* **341:** 797–806.

Ostermann, N., Schlichting, I., Brundiers, R., Konrad, M., Reinstein, J., Veit, T., Goody, R.S., and Lavie, A. 2000. Insights into the phosphoryl-transfer mechanism of human thymidylate kinase gained from crystal structures of enzyme complexes along the reaction coordinate. *Struct. Fold. Des.* **8:** 629–642.

Ostermann, N., Segura-Pena, D., Meier, C., Veit, T., Monnerjahn, C., Konrad, M., and Lavie, A. 2003. Structures of human thymidylate kinase in complex with prodrugs: Implications for the structure-based design of novel compounds. *Biochemistry* **42:** 2568–2577.

Otwinowski, Z. and Minor, W. 1997. Processing of X-ray diffraction data collected in oscillation mode. *Methods Enzymol.* **276:** 307–326.

Peacock, S.J., de Silva, I., and Lowy, F.D. 2001. What determines nasal carriage of *Staphylococcus aureus*? *Trends Microbiol.* **9:** 605–610.

Reinstein, J., Schlichting, I., and Wittinghofer, A. 1990. Structurally and catalytically important residues in the phosphate binding loop of adenylate kinase of *Escherichia coli*. *Biochemistry* **29:** 7451–7459.

Scheffzek, K., Kliche, W., Wiesmuller, L., and Reinstein, J. 1996. Crystal structure of the complex of UMP/CMP kinase from *Dictyostelium discoideum* and the bisubstrate inhibitor P1-(5′-adenosyl) P5-(5′-uridyl) pentaphosphate (UP5A) and Mg^{2+} at 2.2 Å: Implications for water-mediated specificity. *Biochemistry* **35:** 9716–9727.

Segura-Pena, D., Sekulic, N., Ort, S., Konrad, M., and Lavie, A. 2004. Substrate-induced conformational changes in human UMP/CMP kinase. *J. Biol. Chem.* **279:** 33882–33889.

Sekulic, N., Shuvalova, L., Spangenberg, O., Konrad, M., and Lavie, A. 2002. Structural characterization of the closed conformation of mouse guanylate kinase. *J. Biol. Chem.* **277:** 30236–30243.

Stehle, T. and Schulz, G.E. 1990. Three-dimensional structure of the complex of guanylate kinase from yeast with its substrate GMP. *J. Mol. Biol.* **211:** 249–254.

Stuart, D.I., Levine, M., Muirhead, H., and Stammers, D.K. 1979. Crystal structure of cat muscle pyruvate kinase at a resolution of 2.6 Å. *J. Mol. Biol.* **134:** 109–142.

Tian, G.C., Yan, H.G., Jiang, R.T., Kishi, F., Nakazawa, A., and Tsai, M.D. 1990. Mechanism of adenylate kinase. Are the essential lysines essential? *Biochemistry* **29:** 4296–4304.

Vogt, J., Perozzo, R., Pautsch, A., Prota, A., Schelling, P., Pilger, B., Folkers, G., Scapozza, L., and Schulz, G.E. 2000. Nucleoside binding site of herpes simplex type 1 thymidine kinase analyzed by X-ray crystallography. *Proteins* **41:** 545–553.

Vonrhein, C., Schlauderer, G.J., and Schulz, G.E. 1995. Movie of the structural changes during a catalytic cycle of nucleoside monophosphate kinases. *Structure* **3:** 483–490.

Walter, T.S., Diprose, J.M., Mayo, C.J., Siebold, C., Pickford, M.G., Carter, L., Sutton, G.C., Berrow, N.S., Brown, J., Berry, I.M., et al. 2005. A procedure for setting up high-throughput nanolitre crystallization experiments. Crystallization workflow for initial screening, automated storage, imaging and optimization. *Acta Crystallogr. D Biol. Crystallogr.* **61:** 651–657.

Wriggers, W. and Schulten, K. 1997. Protein domain movements: Detection of rigid domains and visualization of hinges in comparisons of atomic coordinates. *Proteins* **29:** 1–14.

Yan, H. and Tsai, M.D. 1999. Nucleoside monophosphate kinases: Structure, mechanism, and substrate specificity. *Adv. Enzymol. Relat. Areas Mol. Biol.* **73:** 103–134.